SIAM J. SCI. COMPUT.
Vol. 40, No. 5, pp. B1229–B1252

LOWEST-ORDER WEAK GALERKIN FINITE ELEMENT METHOD FOR DARCY FLOW ON CONVEX POLYGONAL MESHES*

JIANGGUO LIU†, SIMON TAVENER†, AND ZHUORAN WANG†

Abstract. This paper presents the lowest-order weak Galerkin (WG) finite element method for solving the Darcy equation or elliptic boundary value problems on general convex polygonal meshes. In this approach, constants are used in element interiors and on edges to approximate the primal variable (pressure). The discrete weak gradients of these constant basis functions are established in simple $H(\mathrm{div})$-subspaces on polygons that are explicitly constructed by using the normalized coordinates and Wachspress coordinates [W. Chen and Y. Wang, *Math. Comp.*, 86 (2017), pp. 2053–2087]. These discrete weak gradients are used to approximate the classical gradient in the variational formulation. No penalization is needed for this new method. The method results in symmetric positive-definite sparse linear systems. It is locally mass-conservative and produces continuous normal fluxes. The new method has optimal-order convergence in pressure, velocity, and normal flux, when the convex polygon meshes are shape-regular.

Key words. Darcy flow, elliptic boundary value problems, lowest-order finite element methods, polygonal meshes, Wachspress coordinates, weak Galerkin

AMS subject classifications. 65N15, 65N30, 76S05

DOI. 10.1137/17M1145677

1. Introduction.

This paper concerns finite element methods for elliptic boundary value problems prototyped as

$$\begin{cases} \nabla \cdot (-\mathbf{K}\nabla p) \equiv \nabla \cdot \mathbf{u} = f, & \mathbf{x} \in \Omega, \\ p = p_D, & \mathbf{x} \in \Gamma^D, \\ \mathbf{u} \cdot \mathbf{n} = u_N, & \mathbf{x} \in \Gamma^N, \end{cases} \tag{1}$$

where $\Omega \subset \mathbb{R}^2$ is a bounded (polygonal) domain, p is the unknown primal variable, $\mathbf{K}$ is a 2×2 coefficient matrix that is uniformly symmetric positive-definite, f is a source term, p_D, u_N are, respectively, Dirichlet and Neumann boundary data, and $\mathbf{n}$ is the outward unit normal vector on $\partial\Omega$, which has a nonoverlapping decomposition $\Gamma^D \cup \Gamma^N$.

The elliptic boundary value problem (1) describes Darcy flow when the primal variable p is interpreted as pressure and $\mathbf{K}$ is the hydraulic conductivity. Then the flux $\mathbf{u} = -\mathbf{K}\nabla p$ is understood as velocity and $\mathbf{u} \cdot \mathbf{n}$ is specifically named as normal flux. Heat or electrical conduction in composite materials can also be described by (1), when p is the temperature or electric potential and $\mathbf{K}$ is the thermal or electric conductivity. Accordingly, $\mathbf{u}$ is the heat or electric flux. For ease of presentation, we shall restrict the discussion to the context of Darcy flow.

The elliptic equation (1) can be solved by a variety of finite element methods on simplicial (triangular or tetrahedral) and 2-dim or 3-dim rectangular meshes, e.g.,

*Submitted to the journal's Computational Methods in Science and Engineering section August 31, 2017; accepted for publication (in revised form) July 5, 2018; published electronically September 13, 2018.

http://www.siam.org/journals/sisc/40-5/M114567.html

Funding: The research of the first and third authors was partially supported by NSF DMS-1419077. The second author's research was partially supported by the U.S. National Science Foundation under grant DMS-1720473/1720402.

†Department of Mathematics, Colorado State University, Fort Collins, CO 80523-1874 (liu@math.colostate.edu, tavener@math.colostate.edu, wangz@math.colostate.edu).

the mixed finite element methods [4], the discontinuous Galerkin methods [27], the enhanced Galerkin methods [28], the recently developed weak Galerkin methods [22, 35], and postprocessing procedures [6].

Recently, polygonal and polyhedral meshes have attracted attention from many researchers. Finite element methods, virtual element methods, and mimetic finite difference methods have been developed on these types of meshes for various types of differential equations; the reader is referred to [7, 14, 20, 21, 31, 34] and references therein. Among the methods that can be applied to Darcy flow [5, 13, 15, 17, 30], the local conservation property has been incorporated into the design of methods.

Quadrilaterals and hexahedral meshes, as special polytopal (polygonal or polyhedral) meshes, are attractive for practical tasks of scientific computing, due to their relatively simple data structure and flexibility in accommodating complicated domain geometry. There has been a great deal of research efforts on solving various types of differential equations on quadrilaterals and hexahedral meshes. The Piola transform is used fully [3, 18, 37, 38] or partially [1] to construct $H(\mathrm{div})$-finite elements on quadrilaterals or hexahedra. Based on these, mixed finite element methods can be established for elliptic problems. However, it is unclear whether the methodology of the Piola transform can be applied to polytopes other than quadrilaterals and hexahedra.

Motivated by the importance of the barycentric coordinates to the construction of finite element methods on simplexes, generalized barycentric coordinates such as the Wachspress coordinates have been investigated [19, 32, 33]. For convex polygons, the Wachspress coordinates are nonnegative functions and satisfy the Lagrangian property [9, 19]. Naturally, they can be used as Lagrangian-type basis functions in the continuous Galerkin framework for solving elliptic problems [19]. When this method is applied to Darcy flow computation, however, it is not locally mass-conservative, and it does not produce continuous normal fluxes.

The weak Galerkin (WG) methodology introduced in [35] brings in new perspectives. Degrees of freedom or finite element basis functions are set in element interiors and on element interfaces (edges or faces). New concepts such as discrete weak gradient or divergence or curl are established for these basis functions via integration by parts. Discrete weak gradients (or divergences or curls) are specified in certain spaces that have desired properties and used to approximate the differential operators in variational forms for a variety of problems; see [8, 22, 23, 34] and references therein.

In this paper, we present the novel $\mathrm{WG}(P_0, P_0; CW_0)$ finite element method for Darcy flow or elliptic boundary value problems on convex polygonal meshes. In this approach, the pressure or primal variable is approximated by constant functions in element interiors and on edges, whereas their discrete weak gradients are established in the lowest-order $H(\mathrm{div})$-subspaces on convex polygons that have been recently developed by Chen and Wang in [9]. For convenience, they are denoted as CW_0 in this paper. These discrete weak gradients are used to approximate the classical gradient in the standard variational form for elliptic problems. The rest of this paper presents in detail the finite element scheme for pressure (primal variable), computation of velocity (flux) and normal flux, error analysis, implementation strategies, and numerical results. This new method is also briefly compared with other related methods.

2. Preliminaries. This section presents preliminaries on (i) the Wachspress coordinate functions for polygons and their gradients and curls; (ii) the Chen–Wang $H(\mathrm{div})$-space CW_0 for convex polygons; and (iii) the lowest-order weak Galerkin finite elements $(P_0, P_0; CW_0)$ for convex polygons.

2.1. Wachspress coordinates and their gradients and curls. As is well known, the barycentric coordinates for triangles are simple but useful tools for constructing finite elements. The Wachspress coordinates, investigated in the 1970s and revisited recently in [33], play a similar role for developing finite elements on general polygons. In this subsection, we briefly review the concepts of Wachspress coordinates by following the main ideas in [19].

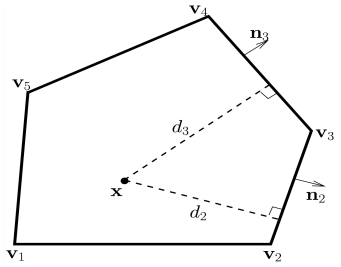

FIG. 1. *A pentagon with quantities needed for computing the Wachspress coordinates.*

Let E be a polygon with n vertices $\mathbf{v}_i (1 \le i \le n)$ that are arranged counterclockwise. Let $\mathbf{n}_i (1 \le i \le n)$ be the outward unit normal vector on edge e_i that connects vertices $\mathbf{v}_i$ and $\mathbf{v}_{i+1}$ (see Figure 1). Here the modulus n convention is adopted for indexing. Let $\mathbf{x} \in E^\circ$ (interior of E). Clearly, its distance to edge e_i is

$$d_i = (\mathbf{v}_i - \mathbf{x}) \cdot \mathbf{n}_i, \qquad 1 \le i \le n. \tag{2}$$

We define a scaled normal vector as

$$\widetilde{\mathbf{n}}_i = \frac{1}{d_i}\mathbf{n}_i, \qquad 1 \le i \le n. \tag{3}$$

Then we define for $1 \le i \le n$,

$$w_i(\mathbf{x}) = \det(\widetilde{\mathbf{n}}_i, \widetilde{\mathbf{n}}_{i+1}), \qquad W(\mathbf{x}) = \sum_{i=1}^{n} w_i(\mathbf{x}). \tag{4}$$

Finally, we define the *Wachspress coordinates* as

$$\lambda_i(\mathbf{x}) = w_i(\mathbf{x})/W(\mathbf{x}), \qquad 1 \le i \le n. \tag{5}$$

For a convex polygon, the Wachspress coordinates are nonnegative and have linear precision; i.e., for $1 \le i \le n$,

$$\lambda_i(\mathbf{x}) \ge 0, \quad \sum_{i=1}^{n} \lambda_i(\mathbf{x}) = 1, \quad \sum_{i=1}^{n} \lambda_i(\mathbf{x})\mathbf{v}_i = \mathbf{x}. \tag{6}$$

The Wachspress coordinates are usually rational functions. For example, if E is a quadrilateral with vertices $(0,0)$, $(1,0)$, (a,b), and $(0,1)$ oriented counterclockwise (see Figure 2), then the Wachspress coordinates are

$$\lambda_i(x,y) = f_i(x,y)/g(x,y), \qquad i = 1,2,3,4, \tag{7}$$

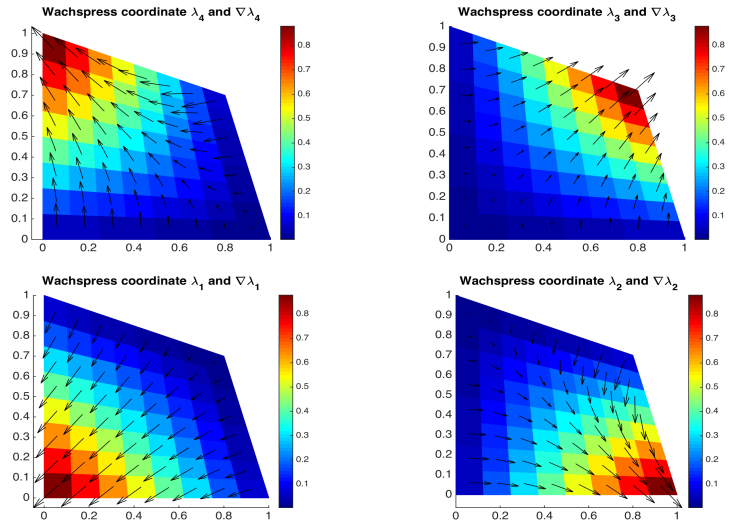

FIG. 2. *The Wachspress coordinate functions and their gradients on a quadrilateral with vertices located at* $(0,0)$, $(1,0)$, $(0.8,0.7)$, *and* $(0,1)$.

where

$$\begin{cases} g(x,y) = ab + b(b-1)x + a(a-1)y, \\ f_1(x,y) = ab + (b(b-1) - ab)x + (a(a-1) - ab)y \\ \qquad\qquad -b(b-1)x^2 + (2ab - a - b + 1)xy - a(a-1)y^2, \\ f_2(x,y) = abx + b(b-1)x^2 - abxy, \\ f_3(x,y) = (a + b - 1)xy, \\ f_4(x,y) = aby - abxy + a(a-1)y^2. \end{cases}$$

Clearly, f_1, f_2, f_3, f_4 are $\mathcal{P}_2$ polynomials and g is a $\mathcal{P}_1$ polynomial. When $a = b = 1$, i.e., the quadrilateral degenerates into the unit square, we have $g(x,y) \equiv 1$ and

$$\lambda_1 = (1-x)(1-y), \quad \lambda_2 = x(1-y,), \quad \lambda_3 = xy, \quad \lambda_4 = (1-x)y,$$

which are bilinear polynomials.

As discussed in [19], one introduces an auxiliary ratio function

$$\mathbf{R}_i(\mathbf{x}) = \frac{\nabla w_i(\mathbf{x})}{w_i(\mathbf{x})}, \qquad 1 \le i \le n. \tag{8}$$

By the quotient rule for differentiation, one is led to

$$\nabla\lambda_i(\mathbf{x}) = \lambda_i(\mathbf{x})\left(\mathbf{R}_i - \sum_{j=1}^{n} \lambda_j \mathbf{R}_j\right), \qquad 1 \le i \le n. \tag{9}$$

Finally, a clockwise 90° rotation of the gradient vector gives

$$\text{curl}(\lambda_i) = \begin{bmatrix} -\partial_y \lambda_i \\ \partial_x \lambda_i \end{bmatrix} = \begin{bmatrix} 0 & -1 \\ 1 & 0 \end{bmatrix} \nabla\lambda_i, \qquad 1 \le i \le n. \tag{10}$$

2.2. Chen–Wang $H(\mathrm{div})$-space CW_0. This type of space is constructed in [9] for general convex polygons and has nice approximation properties.

Let E be a convex polygon as described in subsection 2.1. Let $\mathbf{x}_c = (x_c, y_c)$ be its geometric center and $|E|$ be its area. For $1 \le i \le n$, let $|e_i|$ be the length of edge e_i and $|T_i|$ be the area of the triangle formed by $\mathbf{x}_c, \mathbf{v}_i, \mathbf{v}_{i+1}$.

We will need to calculate some coefficients. First, we define

$$a_i = |e_i|/(2|E|), \qquad 1 \le i \le n. \tag{11}$$

Second, we define

$$b_{i,j} = \delta_{i,j}|e_j| - |e_i||T_j|/|E|, \qquad 1 \le i, j \le n, \tag{12}$$

where $\delta_{i,j}$ is the Kronecker symbol. Third, we define

$$c_{i,j} = -\frac{1}{n}\sum_{k=1}^{n-1} k\, b_{i,j+k}, \qquad 1 \le i, j \le n. \tag{13}$$

It has been shown in [9] that for any $1 \le i, j \le n$,

$$\sum_{n} b_{i,j+k} = 0, \qquad b_{i,j} = c_{i,j} - c_{i,j+1}.$$

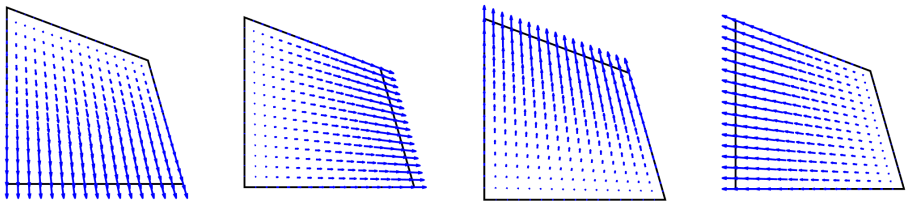

FIG. 3. *The four basis functions for CW_0 on a quadrilateral with vertices located at $(0,0)$, $(1,0)$, $(0.8,0.7)$, and $(0,1)$.*

Basis for CW_0 space. It is shown in [9] that $\dim(CW_0) = n$ and the following n vector-valued functions form a basis for CW_0:

$$\mathbf{w}_i = a_i(\mathbf{x} - \mathbf{x}_c) + \sum_{j=1}^{n} c_{i,j}\,\mathrm{curl}(\lambda_j), \qquad 1 \le i \le n, \tag{14}$$

where λ_j are the Wachspress coordinates discussed in the previous subsection. This set of basis functions relies on the *frame* consisting of the following $(n+1)$ functions:

$$\mathbf{x} - \mathbf{x}_c, \qquad \mathrm{curl}(\lambda_j) \ \ (1 \le j \le n),$$

which utilize the normalized coordinates and the curls of the Wachspress coordinates. The aforementioned coefficients $a_i, c_{i,j}$ form a conversion matrix that has rank n.

Furthermore, there hold that

$$\mathbf{w}_i|_{e_j} \cdot \mathbf{n}_j = \delta_{i,j}, \quad \nabla \cdot \mathbf{w}_i = 2a_i \quad \forall 1 \le i, j \le n. \tag{15}$$

The first item is established in [9]. The second item can be derived from the fact that the divergence of curl is zero. In other words, for these basis functions, the pointwise normal flux on element boundaries and the pointwise divergence on elements are both constants (see Figure 3 for an illustration). These properties make the CW_0 space very attractive for practical applications.

It is worth pointing out that when a polygon degenerates to a triangle or rectangle, CW_0 becomes the standard Raviart–Thomas space RT_0 or $RT_{[0]}$, as expected.

2.3. Weak Galerkin $(P_0, P_0; CW_0)$ finite elements on polygons. In this subsection, we utilize the CW_0 spaces to construct WG finite elements $(P_0, P_0; CW_0)$ on polygons. We follow the approach laid out in [35].

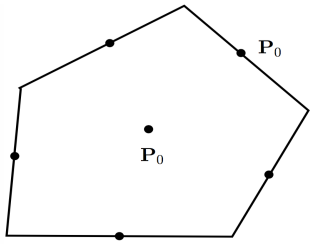

FIG. 4. *WG (P_0, P_0) constant basis functions for the interior and five edges of a pentagon.*

Let E be a polygon. A (P_0, P_0)-type discrete weak function $\phi = \{\phi^\circ, \phi^\partial\}$ on E has two independent pieces: ϕ° is a constant in the polygon interior E°, and ϕ^∂ is a piecewise constant on the edges that make up the polygon boundary E^∂. We specify its discrete weak gradient $\nabla_{w,d}\phi$ in $CW_0(E)$ via integration by parts:

$$\int_E \nabla_{w,d}\phi \cdot \mathbf{w} = \int_{E^\partial} \phi^\partial(\mathbf{w}\cdot\mathbf{n}) - \int_{E^\circ} \phi^\circ(\nabla\cdot\mathbf{w}) \quad \forall \mathbf{w} \in CW_0. \tag{16}$$

So $\nabla_{w,d}\phi$ is a linear combination of those n basis functions of $CW_0(E)$ constructed in (14).

The discrete weak gradient defined in (16) uses exactly both the pointwise normal flux $\mathbf{w}\cdot\mathbf{n}$ and the pointwise divergence $\nabla\cdot\mathbf{w}$ of the vector-valued functions in CW_0. Right here, the two properties in (15) are nicely used.

For an n-gon, there are $(n+1)$ WG basis functions, one for the polygon interior and one for each of the n edges of the polygon. For any such WG basis function $\phi = \{\phi^\circ, \phi^\partial\}$, ϕ° is either 1 or 0, and so is ϕ^∂ on each edge. This indicates that the right-hand side of (16) can be easily evaluated and $\nabla_{w,d}\phi$ can be quickly solved, once the Gram matrix for the CW_0 basis in (14) is computed.

As an example, we consider a pentagon E shown in Figure 4. Let $|E|$ be its area and $|e_i|(i = 1, 2, 3, 4, 5)$ be the length of the ith edge. Let $\phi_0, \phi_1, \phi_2, \phi_3, \phi_4, \phi_5$ be the six WG basis functions that correspond, respectively, to the interior and the five edges of the pentagon. Then the right-hand sides of (16) for these six WG basis functions are, respectively,

$$\begin{bmatrix} -|e_1| \\ -|e_2| \\ -|e_3| \\ -|e_4| \\ -|e_5| \end{bmatrix}, \quad \begin{bmatrix} |e_1| \\ 0 \\ 0 \\ 0 \\ 0 \end{bmatrix}, \quad \begin{bmatrix} 0 \\ |e_2| \\ 0 \\ 0 \\ 0 \end{bmatrix}, \quad \begin{bmatrix} 0 \\ 0 \\ |e_3| \\ 0 \\ 0 \end{bmatrix}, \quad \begin{bmatrix} 0 \\ 0 \\ 0 \\ |e_4| \\ 0 \end{bmatrix}, \quad \begin{bmatrix} 0 \\ 0 \\ 0 \\ 0 \\ |e_5| \end{bmatrix}.$$

Solving the corresponding six size-5 SPD linear systems gives the linear combination coefficients needed for expressing $\nabla_{w,d}\phi_i$ in terms of the basis functions of CW_0.

For a general discussion on weak functions, weak gradient, discrete weak functions, and discrete weak gradients, the reader is referred to [35].

3. Lowest-order WGFEM for Darcy on convex polygonal meshes. Now we establish a new finite element scheme for the Darcy equation by approximating

the pressure by constants in element interiors and on edges. For these constant functions, their discrete weak gradients are calculated in the CW_0 spaces and used to approximate the classical gradient in the variational form.

Let $\mathcal{E}_h$ be a convex polygonal mesh for Ω. For any $E \in \mathcal{E}_h$, we use $|E|$ to denote its area and h_E its diameter. We define $h = \max_{E\in\mathcal{E}_h} h_E$. A polygonal mesh is called shape-regular, provided that it satisfies the following four assumptions.

(A1) *Edges are not too short*. There exists $C_1 > 0$ such that $|e| \geq C_1 h_E$ for any $E \in \mathcal{E}_h$ and any of its edges e.

(A2) *Polygons are not too small*. There exists $C_2 > 0$ such that $|E| \geq C_2 h_E^2$ for any $E \in \mathcal{E}_h$.

(A3) *Interior triangles are not too short*. There exists $C_3 > 0$ such that for any $E \in \mathcal{E}_h$ and any of its edges e, there exists a triangle contained in E with e being its base but the height over e is $\geq C_3 h_E$.

(A4) *Circumscribed triangles are not too tall*. There exists $C_4 > 0$ such that for any $E \in \mathcal{E}_h$, there exists a circumscribed triangle so that the triangle diameter is $\leq C_4 h_E$. Each circumscribed triangle intersects with only a fixed small number of such triangles for other polygons.

Similar definitions can be found in [5, 36].

Let Ω be a polygonal domain equipped with a shape-regular convex polygonal mesh $\mathcal{E}_h$ [36]. Let Γ_h^D be the set of all edges on the Dirichlet boundary Γ^D, and let Γ_h^N be the set of all edges on the Neumann boundary Γ^N. Let S_h be the space of discrete weak functions on $\mathcal{E}_h$ that are degree 0 polynomials (constants) in element interiors and on edges. Let S_h^0 be the subspace of functions in S_h that vanish on Γ_h^D.

To proceed, we define *an L^2-projection* $Q_h = \{Q_h^\circ, Q_h^\partial\}$ such that for any polygon $E \in \mathcal{E}_h$, Q_h° is a local L^2-projection that maps $L^2(E^\circ)$ functions into the space of constant functions on E°, and in the same spirit, Q_h^∂ maps $L^2(E^\partial)$ functions into the space of piecewise constant functions on E^∂. We also define $\mathbf{Q}_h$ as the local L^2-projection from $L^2(E)^2$ to $CW_0(E)$.

WG scheme for pressure on a polygonal mesh. Seek $p_h = \{p_h^\circ, p_h^\partial\} \in S_h$ such that $p_h^\partial|_{\Gamma_h^D} = Q_h^\partial(p_D)$ and

$$\mathcal{A}_h(p_h, q) = \mathcal{F}(q) \qquad \forall q = \{q^\circ, q^\partial\} \in S_h^0, \tag{17}$$

where

$$\mathcal{A}_h(p_h, q) = \sum_{E\in\mathcal{E}_h} \int_E \mathbf{K}\nabla_{w,d} p_h \cdot \nabla_{w,d} q \tag{18}$$

and

$$\mathcal{F}(q) = \sum_{E\in\mathcal{E}_h} \int_E f\, q^\circ - \sum_{e\in\Gamma_h^N} \int_e u_N q^\partial. \tag{19}$$

After a numerical pressure p_h is solved from (17), the elementwise *numerical velocity* is obtained by performing the local L^2-projection back into the subspace CW_0:

$$\mathbf{u}_h = \mathbf{Q}_h(-\mathbf{K}\nabla_{w,d} p_h). \tag{20}$$

But this projection is not needed when $\mathbf{K}$ is an elementwise constant scalar matrix. Then the *bulk normal flux* on an edge is defined as

$$\int_{e\in E^\partial} \mathbf{u}_h \cdot \mathbf{n}_e. \tag{21}$$

Regardless of mesh quality, this new WG finite element scheme possesses two important properties: *local mass conservation* and *normal flux continuity*.

THEOREM 1 (local mass conservation). *Let $E \in \mathcal{E}_h$ be a polygon. Then*

$$\int_E f = \int_{E^\partial} \mathbf{u}_h \cdot \mathbf{n}. \tag{22}$$

Proof. In the finite element scheme (17), take a test function q so that $q|_{E^\circ} = 1$ but it vanishes on all edges and inside all other elements. Then

$$\begin{aligned}\int_E f &= \int_E (\mathbf{K}\nabla_{w,d} p_h) \cdot \nabla_{w,d} q = \int_E \mathbf{Q}_h(\mathbf{K}\nabla_{w,d} p_h) \cdot \nabla_{w,d} q = -\int_E \mathbf{u}_h \cdot \nabla_{w,d} q \\ &= -\int_{E^\partial} q^\partial (\mathbf{u}_h \cdot \mathbf{n}) + \int_{E^\circ} q^\circ (\nabla \cdot \mathbf{u}_h) = \int_{E^\circ} \nabla \cdot \mathbf{u}_h = \int_{E^\partial} \mathbf{u}_h \cdot \mathbf{n}.\end{aligned}$$

It is interesting to note the following:

- The first "=" comes from the WG finite element scheme.
- The second "=" uses the definition of projection $\mathbf{Q}_h$.
- The third "=" uses the definition of numerical velocity.
- The fourth "=" uses the definition of discrete weak gradient.
- The fifth "=" uses the definition of this particular test function q.
- The sixth "=" uses the Gauss divergence theorem on a function in CW_0. ∎

THEOREM 2 (continuity of bulk normal flux). *Let e be an edge shared by two elements E_1, E_2 and $\mathbf{n}_1, \mathbf{n}_2$ be the constant outward unit normal vectors on e, respectively, for E_1, E_2. There holds that*

$$\int_e \mathbf{u}_h^{(1)} \cdot \mathbf{n}_1 + \int_e \mathbf{u}_h^{(2)} \cdot \mathbf{n}_2 = 0. \tag{23}$$

Proof. In the finite element scheme (17), take a test function $q = \{q^\circ, q^\partial\}$ so that the following hold:

- $q^\partial = 1$ only on edge e but $= 0$ on all other edges.
- $q^\circ = 0$ in the interior of any polygonal element.

The definitions of $\mathbf{Q}_h$ and discrete weak gradient together with the Gauss divergence theorem imply that

$$\begin{aligned}0 &= \int_{E_1} (\mathbf{K}\nabla_{w,d} p_h) \cdot \nabla_{w,d} q + \int_{E_2} (\mathbf{K}\nabla_{w,d} p_h) \cdot \nabla_{w,d} q \\ &= \int_{E_1} \mathbf{Q}_h(\mathbf{K}\nabla_{w,d} p_h) \cdot \nabla_{w,d} q + \int_{E_2} \mathbf{Q}_h(\mathbf{K}\nabla_{w,d} p_h) \cdot \nabla_{w,d} q \\ &= \int_{E_1} (-\mathbf{u}_h^{(1)}) \cdot \nabla_{w,d} q + \int_{E_1} (-\mathbf{u}_h^{(2)}) \cdot \nabla_{w,d} q \\ &= -\int_\gamma \mathbf{u}_h^{(1)} \cdot \mathbf{n}_1 q^\partial + \int_{E_1^\circ} \mathbf{u}_h^{(1)} q^\circ - \int_\gamma \mathbf{u}_h^{(2)} \cdot \mathbf{n}_2 q^\partial + \int_{E_2^\circ} \mathbf{u}_h^{(2)} q^\circ \\ &= -\int_\gamma \mathbf{u}_h^{(1)} \cdot \mathbf{n}_1 - \int_\gamma \mathbf{u}_h^{(2)} \cdot \mathbf{n}_2,\end{aligned}$$

which implies the normal continuity of bulk flux. ∎

Errors in pressure, velocity, and normal flux are measured in the following norms:

$$\|p - p_h^\circ\|^2 = \sum_{E \in \mathcal{E}_h} \|p - p_h^\circ\|^2_{L^2(E)}, \tag{24}$$

$$\|\mathbf{u}-\mathbf{u}_h\|^2 = \sum_{E\in\mathcal{E}_h} \|\mathbf{u}-\mathbf{u}_h\|^2_{L^2(E)^2}, \tag{25}$$

$$\|(\mathbf{u}-\mathbf{u}_h)\cdot\mathbf{n}\|^2 = \sum_{E\in\mathcal{E}_h}\sum_{e\subset E^\partial} \frac{|E|}{|e|}\|\mathbf{u}\cdot\mathbf{n}-\mathbf{u}_h\cdot\mathbf{n}\|^2_{L^2(e)}. \tag{26}$$

Here the norm for errors in the normal flux is adopted from [37], which "gives an appropriate scaling of size of $|\Omega|$ for a unit vector."

When convex polygonal meshes are shape-regular and the exact solution has full elliptic regularity, we have first-order accuracy in numerical pressure, velocity, and normal flux as follows:

$$\|p-p_h^\circ\| = \mathcal{O}(h), \quad \|\mathbf{u}-\mathbf{u}_h\| = \mathcal{O}(h), \quad \|(\mathbf{u}-\mathbf{u}_h)\cdot\mathbf{n}\| = \mathcal{O}(h).$$

These results will be stated and proved rigorously in the next section.

4. Error analysis. This section presents error analysis for velocity, normal flux, and pressure for the lowest-order WG scheme (17) with a Dirichlet boundary condition. We adopt the notation $A \lesssim B$ for an inequality $A \le CB$, where C is a positive constant that is independent of mesh size h but may take different values in different appearances. We assume $\mathcal{E}_h$ is a shape-regular convex polygonal mesh.

THEOREM 3. *The WG finite element scheme* (17) *has a unique solution.*

Proof. We follow the approach in [25]. First, we define a seminorm on S_h:

$$|||\phi||| = \sqrt{\mathcal{A}_h(\phi,\phi)} \qquad \forall \phi \in S_h. \tag{27}$$

This seminorm becomes a norm on S_h^0. To see this, we consider $\phi \in S_h^0$ with $|||\phi||| = 0$. Then $\nabla_{w,d}\phi = \mathbf{0}$ on any polygon $E \in \mathcal{E}_h$. For any $\mathbf{w} \in CW_0(E)$, we have

$$(\nabla_{w,d}\phi, \mathbf{w})_E = \langle \phi^\partial, \mathbf{w}\cdot\mathbf{n}\rangle_{E^\partial} - (\phi^\circ, \nabla\cdot\mathbf{w})_{E^\circ} = \langle \phi^\partial - \phi^\circ, \mathbf{w}\cdot\mathbf{n}\rangle_{E^\partial}$$

by applying the definition of discrete weak gradient, integration by parts, and the fact that the classical gradient $\nabla\phi^\circ = \mathbf{0}$. According to the first property in (15), we can choose $\mathbf{w} \in CW_0(E)$ so that $(\mathbf{w}\cdot\mathbf{n})|_e = \phi^\partial|_e - \phi^\circ$ for any edge e of the polygon E. This leads to $\|\phi^\partial|_e - \phi^\circ\|_{L^2(e)} = 0$. Therefore, all the constant values of $\phi = \{\phi^\circ, \phi^\partial\}$ in element interiors and on edges are the same and hence equal to 0, since $\phi \in S_h^0$.

Regarding the solution of the WG finite element scheme (17), it suffices to prove the uniqueness, since this is a linear problem. If $p_h^{(1)}$ and $p_h^{(2)}$ are two solutions of (17), then $e_h = p_h^{(1)} - p_h^{(2)}$ satisfies the following equation:

$$\mathcal{A}_h(e_h, q) = 0 \qquad \forall q \in S_h^0.$$

Since $e_h \in S_h^0$, we can set $q = e_h$ in the above equation to obtain

$$|||e_h|||^2 = \mathcal{A}_h(e_h, e_h) = 0.$$

By the proceeding discussion, we have $e_h \equiv 0$ and hence $p_h^{(1)} \equiv p_h^{(2)}$. ∎

LEMMA 1 (trace inequality for H^1-functions on polygons). *There holds that*

$$\|\eta\|^2_{L^2(e)} \lesssim h^{-1}\|\eta\|^2_{L^2(E)} + h\|\nabla\eta\|^2_{L^2(E)} \qquad \forall \eta \in H^1(E). \tag{28}$$

Proof. See Lemma A.3 in [36]. ∎

LEMMA 2 (approximation capacity of local L^2-projection $\mathbf{Q}_E^c$). *Let $\mathbf{Q}_E^c$ be the L^2-projection that maps $L^2(E)^2$ to the space of constant vectors on E. Then*

$$\|\mathbf{v} - \mathbf{Q}_E^c \mathbf{v}\|_{L^2(E)^2} \lesssim h\|\mathbf{v}\|_{H^1(E)^2} \qquad \forall \mathbf{v} \in H^1(E)^2. \tag{29}$$

Proof. This is derived from Lemma 4.1 in [36] for degree 0 polynomials. ∎

4.1. Approximation properties of CW_0. Approximation properties of the $H(\mathrm{div})$-subspace CW_0 need further examination, since it plays an important role.

LEMMA 3 (approximation capacity of $\mathbf{Q}_h$). *There holds that*

$$\|\mathbf{v} - \mathbf{Q}_h \mathbf{v}\|_{L^2(E)^2} \lesssim h\|\mathbf{v}\|_{H^1(E)^2} \qquad \forall \mathbf{v} \in H^1(E)^2. \tag{30}$$

Proof. This can be proved using the standard techniques in [10]. ∎

We still need a global interpolation operator Π_h that maps $H(\mathrm{div}, \Omega)$ to the global CW_0 space on the entire polygonal mesh $\mathcal{E}_h$. The definition is based on normal trace. Let $E \in \mathcal{E}_h$ be a polygon with edges e_j and outward unit normal vector $\mathbf{n}_j$, $1 \le j \le n$. Let $\mathbf{w}_j (1 \le j \le n)$ be the basis functions in (14). For $\mathbf{v} \in H(\mathrm{div}, \Omega)$, we define

$$f_j = \frac{1}{|e_j|} \int_{e_j} \mathbf{v} \cdot \mathbf{n}_j, \quad \Pi_E \mathbf{v} = \sum_{j=1}^{n} f_j \mathbf{w}_j, \quad (\Pi_h \mathbf{v})|_E = \Pi_E \mathbf{v}. \tag{31}$$

Note that $\Pi_h \mathbf{v} \in H(\mathrm{div}, \Omega)$ also. Applying the Gauss divergence theorem and the above definition for interpolation, we have

$$\int_E \nabla \cdot \Pi_h \mathbf{v} = \int_E \nabla \cdot \Pi_E \mathbf{v} = \int_{E^\partial} (\Pi_E \mathbf{v}) \cdot \mathbf{n} = \int_{E^\partial} \mathbf{v} \cdot \mathbf{n} = \int_E \nabla \cdot \mathbf{v}.$$

In other words, there holds that

$$(\nabla \cdot \Pi_h \mathbf{v}, 1)_E = (\nabla \cdot \mathbf{v}, 1)_E \qquad \forall E \in \mathcal{E}_h. \tag{32}$$

LEMMA 4 (approximation capacity of Π_h). *There holds that*

$$\|\mathbf{v} - \Pi_h \mathbf{v}\|_{L^2(E)^2} \lesssim h\|\mathbf{v}\|_{H^1(E)^2} \qquad \forall \mathbf{v} \in H^1(E)^2. \tag{33}$$

Proof. See Lemma 3.10 in [9]. ∎

LEMMA 5 (trace equivalence for CW_0). *For any $\mathbf{w} \in CW_0$, there holds that*

$$\|\mathbf{w} \cdot \mathbf{n}\|^2_{L^2(E^\partial)} \approx h^{-1} \|\mathbf{w}\|^2_{L^2(E)^2}. \tag{34}$$

Proof. Let $e_i (1 \le i \le n)$ be the edges of E and $\mathbf{w}_i (1 \le i \le n)$ be the CW_0 basis stated in (14). Let $\mathbf{w} = \sum_{i=1}^n c_i \mathbf{w}_i$. It is proved in Lemma 3.7 of [9] that $\|\mathbf{w}_i\|_{L^2(E)^2} \lesssim |e_i|$. So we have, by triangle inequalities,

$$\|\mathbf{w}\|^2_{L^2(E)^2} = \left\| \sum_{i=1}^n c_i \mathbf{w}_i \right\|^2_{L^2(E)^2} \lesssim \sum_{i=1}^n |c_i|^2 \|\mathbf{w}_i\|^2_{L^2(E)^2} \lesssim \sum_{i=1}^n |c_i|^2 |e_i|^2.$$

On the other hand, by (15), we have $\mathbf{w}|_{e_i} \cdot \mathbf{n}_i = c_i$, and hence

$$\|\mathbf{w} \cdot \mathbf{n}\|^2_{L^2(E^\partial)} = \sum_{i=1}^n |c_i|^2 |e_i|.$$

The mesh is shape-regular, so $h^{-1} e_i \approx \text{const}$, and thus $h^{-1} \|\mathbf{w}\|^2_{L^2(E)^2} \lesssim \|\mathbf{w} \cdot \mathbf{n}\|^2_{L^2(E^\partial)}$. The other inequality follows from the standard techniques. ∎

4.2. Approximation properties of discrete weak gradients. We establish some lemmas in this subsection.

LEMMA 6. *Let E be a polygon. For any $p \in H^1(E)$, there holds that*

$$\mathbf{Q}_h(\nabla p) = \nabla_{w,d}(Q_h p). \tag{35}$$

The above commuting identity along with the diagram in Figure 5 *indicates that the discrete weak gradient indeed provides a nice approximation of the classical gradient. In Figure* 5*, $WG(P_0, P_0)$ refers to the elementwise WG finite element space of discrete weak functions that are constants in the element interior and also constants on each edge.*

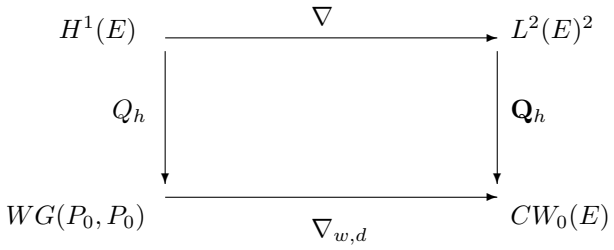

FIG. 5. *Commuting diagram for operators.*

Proof. Consider any $\mathbf{w} \in CW_0(E)$. Applying integration by parts and the definition of discrete weak gradient, we have

$$\begin{aligned}\int_E \mathbf{Q}_h(\nabla p)\cdot\mathbf{w} &= \int_E \nabla p\cdot\mathbf{w} = \int_{E^\partial} p(\mathbf{w}\cdot\mathbf{n}) - \int_{E^\circ} p(\nabla\cdot\mathbf{w})\\ &= \int_{E^\partial}(Q_h^\partial p)(\mathbf{w}\cdot\mathbf{n}) - \int_{E^\circ}(Q_h^\circ p)(\nabla\cdot\mathbf{w}) = \int_E \nabla_{w,d}(Q_h p)\mathbf{w}.\end{aligned}$$

The desired identity follows from the arbitrariness of the test function $\mathbf{w}$. ∎

LEMMA 7. *For any $\mathbf{v} \in H(\mathrm{div}, \Omega)$ and any $\phi = \{\phi^\circ, \phi^\partial\} \in S_h^0(\mathcal{E}_h)$, there holds that*

$$\sum_{E\in\mathcal{E}_h}(\nabla\cdot\mathbf{v}, \phi^\circ)_E = -\sum_{E\in\mathcal{E}_h}(\Pi_h\mathbf{v}, \nabla_{w,d}\phi)_E. \tag{36}$$

Proof. By (32) and the definition of $\nabla_{w,d}$, we have

$$\sum_{E\in\mathcal{E}_h}(\nabla\cdot\mathbf{v}, \phi^\circ)_E = \sum_{E\in\mathcal{E}_h}(\nabla\cdot\Pi_h\mathbf{v}, \phi^\circ)_E = \sum_{E\in\mathcal{E}_h}(\Pi_h\mathbf{v}\cdot\mathbf{n}, \phi^\partial)_{E^\partial} - \sum_{E\in\mathcal{E}_h}(\Pi_h\mathbf{v}, \nabla_{w,d}\phi)_E.$$

The desired equality follows from the normal continuity of $\Pi_h\mathbf{v}$ across edges. ∎

4.3. Error equation. This subsection examines the error between the L^2-projection of the exact solution and the finite element solution.

LEMMA 8 (error equation). *For the exact solution p of* (1) *and the numerical solution p_h of* (17)*, there holds that*

$$\mathcal{A}_h(p_h - Q_h p, q) = \sum_{E\in\mathcal{E}_h}\Big(\Pi_h(\mathbf{K}\nabla p) - \mathbf{K}\mathbf{Q}_h(\nabla p), \nabla_{w,d}q\Big)_E \quad \forall q \in S_h^0(\mathcal{E}_h). \tag{37}$$

Proof. On the one hand, since $-\mathbf{K}\nabla p \in H(\mathrm{div}, \Omega)$, we have by Lemma 7 that

$$\mathcal{A}_h(p_h, q) = \sum_{E\in\mathcal{E}_h} (f, q^\circ)_E = \sum_{E\in\mathcal{E}_h} (\nabla\cdot(-\mathbf{K}\nabla p), q^\circ)_E = \sum_{E\in\mathcal{E}_h} (\Pi_h(\mathbf{K}\nabla p), \nabla_{w,d} q)_E.$$

On the other hand, we have by Lemma 6 that

$$\mathcal{A}_h(Q_h p, q) = \sum_{E\in\mathcal{E}_h} (\mathbf{K}\nabla_{w,d}(Q_h p), \nabla_{w,d} q)_E = \sum_{E\in\mathcal{E}_h} (\mathbf{K}\mathbf{Q}_h(\nabla p), \nabla_{w,d} q)_E.$$

Subtraction of the above two equalities yields the claimed error equation. ∎

LEMMA 9 (difference between L^2-projection and finite element solution). *Let p be the exact solution of* (1). *Assume that $p \in H^2(\Omega)$ and $-\mathbf{K}\nabla p \in H^1(\Omega)^2$. Then*

$$\|\nabla_{w,d}(p_h - Q_h p)\|_{L^2(\Omega)} \lesssim h. \tag{38}$$

Proof. Let $e_h = p_h - Q_h p$. Since $\mathbf{K}$ is SPD globally, there exists a constant $\alpha > 0$ such that

$$\mathcal{A}_h(e_h, e_h) = \sum_{E\in\mathcal{E}_h} (\mathbf{K}\nabla_{w,d} e_h, \nabla_{w,d} e_h) \geq \alpha \|\nabla_{w,d} e_h\|^2_{L^2(\Omega)}.$$

On the other hand, taking $q = e_h$ in the error equation (37) and applying the Cauchy–Schwarz inequality, we obtain

$$\mathcal{A}_h(e_h, e_h) \leq \sum_{E\in\mathcal{E}_h} \|\Pi_h(\mathbf{K}\nabla p) - \mathbf{K}\mathbf{Q}_h(\nabla p)\|_{L^2(E)^2} \|\nabla_{w,d} e_h\|_{L^2(E)^2}.$$

Since $\Pi_h(\mathbf{K}\nabla p)$ and $\mathbf{K}\mathbf{Q}_h(\nabla p)$ both approximate $\mathbf{K}\nabla p$, we consider their performances separately and then apply a triangle inequality. The assumptions imply

$$\|\Pi_h(\mathbf{K}\nabla p) - \mathbf{K}\nabla p\|_{L^2(E)^2} \lesssim h \|\mathbf{K}\nabla p\|_{H^1(E)^2},$$

$$\|\mathbf{K}\nabla p - \mathbf{K}\mathbf{Q}_h(\nabla p)\|_{L^2(E)^2} \lesssim h \|\mathbf{K}\|_{L^\infty(E)} \|\nabla p\|_{H^1(E)^2}.$$

By summing the above elementwise estimates, we obtain

$$\|\Pi_h(\mathbf{K}\nabla p) - \mathbf{K}\mathbf{Q}_h(\nabla p)\|_{L^2(\Omega)^2} \lesssim h,$$

and then

$$\alpha \|\nabla_{w,d} e_h\|^2_{L^2(\Omega)} \leq \mathcal{A}_h(e_h, e_h) \lesssim h \|\nabla_{w,d} e_h\|_{L^2(\Omega)}.$$

The claimed result comes after a multiplicative cancellation. ∎

4.4. Error analysis for velocity and normal flux. We present error analysis for velocity based on the error equation. Then we use trace inequalities to derive an error estimate for normal flux.

THEOREM 4 (convergence in velocity). *Assume the exact solution of* (1) *has regularity $p \in H^2(\Omega)$ and $\mathbf{u} \in H^1(\Omega)^2$. Let $\mathbf{u}_h$ be the numerical velocity obtained from* (20). *Then*

$$\|\mathbf{u} - \mathbf{u}_h\| \lesssim h. \tag{39}$$

Proof. This will be established by using CW_0 approximation capacity and the error equation.

Step 1. On each element, by Lemmas 6 and 3, we have

$$\begin{aligned}\|\mathbf{K}\nabla p - \mathbf{K}\nabla_{w,d}(Q_h p)\|_{L^2(E)^2} &= \|\mathbf{K}\nabla p - \mathbf{K}\mathbf{Q}_h(\nabla p)\| \\ &\le \|\mathbf{K}\|_{L^\infty(E)}\|\nabla p - \mathbf{Q}_h(\nabla p)\|_{L^2(E)^2} \lesssim h.\end{aligned}$$

Step 2. By the approximation capacity of $\mathbf{Q}_h$, we have elementwise

$$\|\mathbf{K}\nabla_{w,d}(Q_h p) - \mathbf{Q}_h(\mathbf{K}\nabla_{w,d}(Q_h p))\| \lesssim h.$$

Step 3. By the stability of $\mathbf{Q}_h$ and Lemma 9, we have

$$\begin{aligned}\|\mathbf{Q}_h(\mathbf{K}\nabla_{w,d}(Q_h p)) - \mathbf{Q}_h(\mathbf{K}\nabla_{w,d} p_h)\| &\le \|\mathbf{K}\nabla_{w,d}(Q_h p) - \mathbf{K}\nabla_{w,d} p_h\| \\ &\le \|\mathbf{K}\|_{L^\infty}\|\nabla_{w,d}(Q_h p) - \nabla_{w,d} p_h\|_{L^2(E)^2} \lesssim h.\end{aligned}$$

Then (39) follows from summation over the mesh and triangle inequalities. ∎

THEOREM 5 (convergence in normal flux). *Assume the exact solution of* (1) *has regularity* $p \in H^2(\Omega)$ *and* $\mathbf{u} \in H^1(\Omega)^2$. *Let* $\mathbf{u}_h$ *be the numerical velocity obtained from* (20). *Then*

$$\|\mathbf{u}\cdot\mathbf{n} - \mathbf{u}_h\cdot\mathbf{n}\| \lesssim h. \tag{40}$$

Proof. Let $E \in \mathcal{E}_h$. By a triangle inequality, we have

$$\|(\mathbf{u}-\mathbf{u}_h)\cdot\mathbf{n}\|^2_{L^2(E^\partial)} \lesssim \|(\mathbf{u}-\Pi_h\mathbf{u})\cdot\mathbf{n}\|^2_{L^2(E^\partial)} + \|(\Pi_h\mathbf{u}-\mathbf{u}_h)\cdot\mathbf{n}\|^2_{L^2(E^\partial)} =: \mathrm{I}+\mathrm{II}. \tag{41}$$

For I, we utilize $\mathbf{c} = \mathbf{Q}_h^c\mathbf{u}$ studied in Lemma 2. Clearly, $\Pi_h(\mathbf{Q}_h^c\mathbf{u}) = \mathbf{Q}_h^c(\mathbf{u})$. By the two trace inequalities in Lemma 1 (vector version) and Lemma 5, we have

$$\begin{aligned}I &\lesssim \|(\mathbf{u}-\mathbf{c})\cdot\mathbf{n}\|^2_{L^2(E^\partial)} + \|\Pi_h(\mathbf{u}-\mathbf{c})\cdot\mathbf{n}\|^2_{L^2(E^\partial)} \\ &\lesssim h^{-1}\|\mathbf{u}-\mathbf{c}\|^2_{L^2(E)^2} + h|\mathbf{u}-\mathbf{c}|^2_{H^1(E)^2} + h^{-1}\|\Pi_h(\mathbf{u}-\mathbf{c})\|^2_{L^2(E)^2} \\ &\lesssim h\|\mathbf{u}\|^2_{H^1(E)^2} + h|\mathbf{u}|^2_{H^1(E)^2} + h\|\mathbf{u}\|^2_{H^1(E)^2}.\end{aligned} \tag{42}$$

For the last step, we have used Lemma 2 and Lemma 3.8 in [9].

For II, we apply Lemma 5, a triangle inequality, and Lemma 4 to obtain

$$\begin{aligned}\mathrm{II} &\approx h^{-1}\|\Pi_h\mathbf{u}-\mathbf{u}_h\|^2_{L^2(E)^2} \lesssim h^{-1}(\|\Pi_h\mathbf{u}-\mathbf{u}\|^2_{L^2(E)^2} + \|\mathbf{u}-\mathbf{u}_h\|^2_{L^2(E)^2}) \\ &\lesssim h\|\mathbf{u}\|^2_{H^1(E)^2} + h^{-1}\|\mathbf{u}-\mathbf{u}_h\|^2_{L^2(E)^2}.\end{aligned} \tag{43}$$

Summing (42), (43) over the mesh, using the fact that $|E|/|e| \approx h$, the norm definition (26), and Theorem 4, we finally obtain the claimed result in Theorem 5. ∎

4.5. Error analysis for pressure. This is based on a duality argument.

THEOREM 6 (convergence in pressure). *Assume the exact solution* p *of* (1) *has regularity* $p \in H^2(\Omega)$ *and* $\mathbf{u} \in H^1(\Omega)^2$. *There holds that*

$$\|p - p_h^\circ\| \lesssim h. \tag{44}$$

Proof. From the triangle inequality,

$$\|p - p_h^\circ\| \le \|p - Q_h^\circ p\| + \|Q_h^\circ p - p_h^\circ\|, \tag{45}$$

and the approximation capacity,

$$\|p - Q_h^\circ p\| \lesssim h\|p\|_{H^1(\Omega)}, \tag{46}$$

it is clear that we need an estimate on $\|p_h^\circ - Q_h^\circ p\|_{L^2(\Omega}$. This will be done by a duality argument. For convenience, we set $e_h = p_h - Q_h p$. Note that $p_h^\partial = Q_h^\partial(p_D)$ on $\Gamma = \partial\Omega$ and hence $e_h \in S_h^0(\mathcal{E}_h)$.

We consider the dual problem

$$\nabla \cdot (-\mathbf{K}\nabla\phi) = e_h^\circ, \qquad \phi|_{\partial\Omega} = 0. \tag{47}$$

Assume ϕ has also full elliptic regularity, specifically

$$\|\phi\|_{H^2(\Omega)} \lesssim \|e_h^\circ\|_{L^2(\Omega)}. \tag{48}$$

By Lemmas 7 and 6 and the definition of $\mathbf{Q}_h$, we have

$$\begin{aligned}
\|e_h^\circ\|^2 &= (e_h^\circ, e_h^\circ) = (\nabla\cdot(-\mathbf{K}\nabla\phi), e_h^\circ) = (\Pi_h(\mathbf{K}\nabla\phi), \nabla_{w,d} e_h) \\
&= (\Pi_h(\mathbf{K}\nabla\phi), \nabla_{w,d} p_h - \mathbf{Q}_h(\nabla p)) \\
&= (\Pi_h(\mathbf{K}\nabla\phi), \nabla_{w,d} p_h - \nabla p) \\
&= (\Pi_h(\mathbf{K}\nabla\phi) - \mathbf{K}\nabla\phi, \nabla_{w,d} p_h - \nabla p) + (\mathbf{K}\nabla\phi, \nabla_{w,d} p_h - \nabla p).
\end{aligned} \tag{49}$$

Let us pause to look at what we are dealing with and what tools we have:

- For the direct problem, we need to estimate

$$\nabla p - \nabla_{w,d} p_h, \qquad \mathbf{K}\nabla p - \mathbf{Q}_h(\mathbf{K}\nabla p).$$

- For the dual problem, we need to estimate

$$\nabla\phi - \mathbf{Q}_h(\nabla\phi), \qquad \mathbf{K}\nabla\phi - \Pi_h(\mathbf{K}\nabla\phi).$$

- For pressure, we have the local L^2-projection $Q_h = \{Q_h^\circ, Q_h^\partial\}$.
- For gradient, we have the local $\mathbf{L}^2$-projection $\mathbf{Q}_h$.
- For velocity, we have $\mathbf{Q}_h$ and the global interpolation Π_h.
- The commuting diagram (Lemma 6) is useful for making connections.

Now we continue and use Lemma 6 to obtain

$$\begin{aligned}
(\mathbf{K}\nabla\phi, \nabla_{w,d} p_h - \nabla p) &= (\mathbf{K}\nabla\phi, \nabla_{w,d} p_h) - (\mathbf{K}\nabla\phi, \nabla p) \\
&= (\mathbf{K}(\nabla\phi - \mathbf{Q}_h(\nabla\phi)), \nabla_{w,d} p_h) + (\mathbf{K}\nabla_{w,d}(Q_h\phi), \nabla_{w,d} p_h) - (\mathbf{K}\nabla\phi, \nabla p).
\end{aligned} \tag{50}$$

Next we utilize the self-adjointness of $\mathbf{K}$ and the orthogonality implied by $\mathbf{Q}_h$ to get

$$\begin{aligned}
&(\mathbf{K}(\nabla\phi - \mathbf{Q}_h(\nabla\phi)), \nabla_{w,d} p_h) \\
&\quad = (\mathbf{K}(\nabla\phi - \mathbf{Q}_h(\nabla\phi)), \nabla_{w,d} p_h - \nabla p) + (\mathbf{K}(\nabla\phi - \mathbf{Q}_h(\nabla\phi)), \nabla p) \\
&\quad = (\mathbf{K}(\nabla\phi - \mathbf{Q}_h(\nabla\phi)), \nabla_{w,d} p_h - \nabla p) + (\nabla\phi - \mathbf{Q}_h(\nabla\phi), \mathbf{K}\nabla p) \\
&\quad = (\mathbf{K}(\nabla\phi - \mathbf{Q}_h(\nabla\phi)), \nabla_{w,d} p_h - \nabla p) \\
&\qquad + (\nabla\phi - \mathbf{Q}_h(\nabla\phi), \mathbf{K}\nabla p - \mathbf{Q}_h(\mathbf{K}\nabla p)).
\end{aligned} \tag{51}$$

Putting (49), (50), (51) together, we have

$$
\begin{aligned}
\|e_h^\circ\|^2 &= \Big(\mathbf{K}\nabla\phi - \Pi_h(\mathbf{K}\nabla\phi), \nabla p - \nabla_{w,d} p_h\Big) \\
&\quad - \Big(\mathbf{K}(\nabla\phi - \mathbf{Q}_h(\nabla\phi)), \nabla p - \nabla_{w,d} p_h\Big) \\
&\quad + \Big(\mathbf{K}\nabla p - \mathbf{Q}_h(\mathbf{K}\nabla p), \nabla\phi - \mathbf{Q}_h(\nabla\phi)\Big) \\
&\quad - \Big((\mathbf{K}\nabla\phi, \nabla p) - (\mathbf{K}\nabla_{w,d}(Q_h\phi), \nabla_{w,d} p_h)\Big) \\
&=: T_1 + T_2 + T_3 + T_4.
\end{aligned} \tag{52}
$$

By a triangle inequality and Lemmas 6, 3, and 9, we have

$$
\|\nabla p - \nabla_{w,d} p_h\| \le \|\nabla p - \mathbf{Q}_h(\nabla p)\| + \|\nabla_{w,d}(Q_h p) - \nabla_{w,d} p_h\| \lesssim h. \tag{53}
$$

By the lemmas on the approximation capacity of Π_h and $\mathbf{Q}_h$ and the assumption on dual solution regularity, we have

$$
\begin{aligned}
&\|\mathbf{K}\nabla\phi - \Pi_h(\mathbf{K}\nabla\phi)\| \lesssim h\|\mathbf{K}\nabla\phi\|_{H^1} \lesssim h\|\mathbf{K}\|\|\phi\|_{H^2} \lesssim h\|\mathbf{K}\|\|e_h^\circ\|, \\
&\|\nabla\phi - \mathbf{Q}_h(\nabla\phi)\| \lesssim h\|\nabla\phi\|_{H^1} \lesssim h\|\phi\|_{H^2} \lesssim h\|e_h^\circ\|, \\
&\|\nabla p - \mathbf{Q}_h(\nabla p)\| \lesssim h\|\nabla p\|_{H^1} \lesssim h\|p\|_{H^2}, \\
&\|\mathbf{K}\nabla p - \mathbf{Q}_h(\mathbf{K}\nabla p)\| \lesssim h\|\mathbf{K}\nabla p\|_{H^1} \approx h\|\mathbf{u}\|_{H^1}.
\end{aligned} \tag{54}
$$

Accordingly, the Cauchy–Schwarz inequality and (53), (54) together imply

$$
|T_1| \lesssim h^2\|e_h^\circ\|, \quad |T_2| \lesssim h^2\|e_h^\circ\|, \quad |T_3| \lesssim h^2\|e_h^\circ\|. \tag{55}
$$

For T_4, by the self-adjointness of $\mathbf{K}$, the orthogonality implied by Q_h°, the variational form, and the finite element scheme, we have

$$
\begin{aligned}
T_4 &= (\mathbf{K}\nabla\phi, \nabla p) - (\mathbf{K}\nabla_{w,d}(Q_h\phi), \nabla_{w,d} p_h) \\
&= (\mathbf{K}\nabla p, \nabla\phi) - (\mathbf{K}\nabla_{w,d} p_h, \nabla_{w,d}(Q_h\phi)) \\
&= (f,\phi) - (f, Q_h^\circ\phi) = (f, \phi - Q_h^\circ\phi) = (f - Q_h^\circ f, \phi - Q_h^\circ\phi).
\end{aligned} \tag{56}
$$

Therefore,

$$
\begin{aligned}
|T_4| &\le \|f - Q_h^\circ f\|\|\phi - Q_h^\circ\phi\| \lesssim \|f - Q_h^\circ f\| h\|\nabla\phi\|_{H^1(\Omega)^2} \\
&\lesssim h\|f - Q_h^\circ f\|\|e_h^\circ\|.
\end{aligned} \tag{57}
$$

Now (52), (55), (57) together imply $\|e_h^\circ\| \lesssim h$. Combined with the projection error $\mathcal{O}(h)$ in (46), this leads finally to (44), the claimed estimate in Theorem 6. ∎

Here are some remarks:

(i) The above analysis shows that the error $e_h^\circ = p_h^\circ - Q_h^\circ p$ is dictated by term T_4, for which $\|f - Q_h^\circ f\|$ is a determining factor. When f has sufficient regularity, e.g., $f \in H^1(\Omega)$, we have *superconvergence* $e_h^\circ = \mathcal{O}(h^2)$. This shall be numerically illustrated in section 7.

(ii) Note that for this WG method, a first-order convergence in pressure can be attained for problems without full elliptic regularity; see, e.g., Example 2 in [24]. We omit the details here.

5. Other related methods. Five other types of finite element methods are tightly related to the new WG method developed in this paper:

(i) the mixed finite element method (CW_0, P_0) presented in [9];
(ii) the WG$(Q_0, Q_0; RT_{[0]})$ method on quadrilateral meshes in our recent work [24] and the WG$(P_1, P_0; P_0^2)$ method with stabilization derived from [25];
(iii) the continuous Galerkin method studied in [19], which uses the Wachspress coordinates directly;
(iv) the hybrid high-order (HHO) methods [12];
(v) the mimetic finite difference (MFD) methods [5, 15].

MFEM$(\boldsymbol{CW_0, P_0})$. As investigated in [9], the CW_0 subspace on a polygon can be paired directly with the P_0 subspace on the same polygon to form a mixed finite element method for solving elliptic problems. Although the element pair (CW_0, P_0) satisfies the inf-sup condition and hence is stable, an indefinite linear system needs to be solved after the finite element discretization. Hybridization can be employed to convert the saddle-point problems into definite problems.

The WG method in this paper is related to but different from the mixed method in [9]. Our WG method is based on the primal variational formulation, has pressure unknowns in element interiors and on edges, and results in a symmetric positive-definite discrete system. Moreover, in our WG method, Dirichlet conditions are essential and Neumann conditions are natural, whereas it is the other way around in the mixed method.

WG$(\boldsymbol{Q_0, Q_0; RT_{[0]}})$ on quadrilateral or hybrid meshes. Actually, the WG method in our recent work [24] treats triangular, rectangular, quadrilateral, and hybrid meshes in a unified way. Rectangular meshes are naturally a special case of quadrilateral meshes. A hybrid mesh consists of quadrilaterals and triangles. In any case, pressure is approximated by constants inside the elements and on edges, similar to the method in this paper.

In [24], the discrete weak gradients of these constant functions are specified in the standard local RT_0 spaces for triangles or the unmapped local $RT_{[0]}$ spaces for quadrilaterals. These Raviart–Thomas spaces consist of polynomial vectors and hence are easier to implement. Regardless of mesh quality, the WG method in [24] is locally conservative and produces continuous normal fluxes. An *asymptotically parallelogram quadrilateral* mesh assumption is placed to guarantee optimal convergence in pressure, velocity, and normal flux. According to [2, 24], for asymptotically parallelogram quadrilateral meshes, the angles between the outward normals on the opposite edges are close to π. Although any polygonal domain can be partitioned into such meshes [2, 39], there are applications for which rough quadrilateral or polygonal meshes need to be used [5, 37]. The WG method in this paper is applicable to more general (shape-regular) polygonal meshes. There is no restriction for quadrilaterals to be asymptotically parallelogram. However, the CW_0 vector-valued functions are rational functions. A frame needs to be used to get the basis functions. An apparent benefit is the first-order convergence in pressure, velocity, and normal flux for any shape-regular convex polygonal meshes.

The WG methods in [24] and this paper are both lowest order (using constant approximants) and share the same spirit that no stabilization is needed.

WG$(\boldsymbol{P_1, P_0; P_0^2})$ having stabilization. The family of stabilized WG$(P_{k+1}, P_k; P_k^d)$ finite element schemes (dimension $d = 2, 3$) developed in [25] are for polytopal meshes. The case $k = 0$, $d = 2$, i.e., WG$(P_1, P_0; P_0^2)$, is closely related to the WG scheme in this paper. The WG$(P_1, P_0; P_0^2)$ finite element scheme for elliptic problems

can be described as follows. Let $\mathcal{E}_h$ be a polygonal mesh, and define

$$\mathcal{B}_h(p_h, q) = \mathcal{A}_h(p_h, q) + \mathcal{S}_h(p_h, q), \tag{58}$$

where $\mathcal{A}_h(p_h, q)$ has the same form as the one shown in (18) but is defined for shape functions that are linear polynomials in element interiors and constants on edges. Of course, their discrete weak gradients are in P_0^2. Here $\mathcal{S}_h$ is a stabilization term:

$$\mathcal{S}_h(p_h, q) = \rho \sum_{E\in\mathcal{E}_h} \sum_{e\subset E^\partial} h_E^{-1} \langle Q_h^\partial(p_h^\circ) - p_h^\partial, Q_h^\partial(q^\circ) - q^\partial \rangle_e, \tag{59}$$

and Q_h^∂ is the local L^2-projection into the P_0 space on an edge.

It has been proved in [25] that these stabilized WG schemes are locally mass-conservative and produce continuous normal fluxes, which depend on the penalty factor ρ. However, how to compute a numerical velocity was not discussed in [25], and hence further study is needed. One possible procedure for postprocessing is to apply an interpolation operator to the normal fluxes on the edges to obtain a numerical velocity in the CW_0 space. For $\rho > 0$, the schemes are stable and possess optimal-order convergence in pressure. So the suggested choice is $\rho = 1$. If other factors are to be considered, e.g., the discrete maximum principle, then an optimal value for ρ could be problem dependent.

Continuous Galerkin method based on Wachspress coordinates. In this approach [19], the Wachspress coordinates are naturally used as node-oriented basis functions due to their Lagrangian properties. This method has the fewest degrees of freedom. The analysis on their gradient bounds in [19] guarantees the stability and optimal convergence of this method. However, this method is in general not locally conservative and does not produce continuous normal fluxes, similar to other traditional CG methods on triangular and rectangular meshes.

HHO method. It is interesting to observe some similarities and differences between our WG method and the HHO method [12]. Both methods use basis functions in element interiors and on edges. For HHO, on each individual element, these two types of polynomial basis functions together are lifted to higher-order polynomials (the third type) through solving a local Neumann problem. Then the gradients of the third-type basis functions are used to approximate the classical gradient in the variational formulation. However, for WG, on an individual element, these two types of polynomial basis functions are used to construct discrete weak gradients through integration by parts. These discrete weak gradients are used to approximate the classical gradient in the variational formulation.

MFD methods. The MFD methods [5, 15] (and references therein) are also popular. When applied to the Darcy or elliptic equation, the MFD method approximates the pressure and normal flux simultaneously by using two discrete spaces (one for pressure and one for normal flux). The discrete divergence operator and the discrete flux operator are defined to approximate the corresponding continuous operators. These two discrete operators are adjoint to each other.

A major difference between our WG method and the MFD methods lies in that of primal and mixed formulations. Our WG method relies on the primal formulation, approximates the pressure in element interiors and on edges, and produces its discrete weak gradient and then approximates velocity. The MFD methods inherit the spirit of mixed formulation by approximating pressure and velocity at the same time.

One commonality between the MFD and WG methods is the use of duality or adjointness of operators. For WG, the definition of a discrete weak gradient operator

relies on the duality of the classical divergence operator. For MFD, the discrete divergence operator is defined first, and then the discrete flux operator is defined as its adjoint [5, 15].

Others. The similarities and differences between the WG methods and the hybridizable discontinuous Galerkin (HDG) methods were commented on in [11, 26]. Here we make a further comment that the WG methodology establishes approximation of the classical (gradient, curl, div, etc.) differential operators by discrete weak operators. This is accomplished through integration by parts utilizing the WG basis functions defined in element interiors and those on interelement boundaries. Our WG method in this paper is based on an approximation of the classical gradient by the discrete weak gradient in the CW_0 space and hence fits in the abstract framework of gradient schemes investigated in [16]. But an elaboration on this is omitted due to page limitation.

6. Implementation. This section discusses efficient implementation strategies for the WG$(P_0, P_0; CW_0)$ solver. For ease of implementation, we assume $\mathbf{K}$ is a constant 2×2 SPD matrix on each element. This can be achieved by taking elementwise averages.

(0) Generating polygonal meshes. The quality of polygonal meshes determines performance of finite element solvers on such meshes. For the numerical experiments in this paper, we use `PolyMesher` [29], which is readily available in MATLAB. Quadrilateral meshes are treated as a special type of polygonal meshes.

(1) Computing $\boldsymbol{\lambda_j}$, curl$(\boldsymbol{\lambda_j})$. The new ingredients in this solver are the Wachspress coordinates λ_j and their gradients and curls. These quantities can be calculated using the formulas presented in subsection 2.1.

(2) Frame and basis for elementwise $\boldsymbol{CW_0}$ space. As discussed in subsection 2.1, on each polygonal element, we use the normalized coordinates and the curls of the Wachspress coordinates

$$\mathbf{x} - \mathbf{x}_c, \qquad \operatorname{curl}(\lambda_j) \ \ (j = 1, \ldots, n)$$

to first form a frame for CW_0. Then the conversion matrix (see subsection 2.2) is used to obtain the values of the CW_0 basis functions $\mathbf{w}_i (1 \le i \le n)$.

(3) Computing Gram matrix $\boldsymbol{G(\mathbf{w}_1, \ldots, \mathbf{w}_n)}$ for $\boldsymbol{CW_0}$ basis. This can be done straightforwardly by employing a Gaussian quadrature on each element. Notice that the formulas for $\lambda_j, \operatorname{curl}(\lambda_j)$ do not apply directly when a point is on the boundary of a polygon. So a Gaussian quadrature indeed avoids unnecessary complexity.

The Gram matrix is used in computing discrete weak gradients; see formula (16).

(4) Computing weighted Gram matrix $\boldsymbol{G_{\mathbf{K}}(\mathbf{w}_1, \ldots, \mathbf{w}_n)}$. Recall that

$$G_{\mathbf{K}} = \left[\int_E \mathbf{w}_i \cdot (\mathbf{K}\mathbf{w}_j) \right]_{1 \le i,j \le n} \tag{60}$$

is used in computing an elementwise stiffness matrix. A Gaussian quadrature applies.

(5) Computing projection $\mathbf{Q}_h(\mathbf{K}\mathbf{w}_j)$. Suppose

$$\mathbf{Q}_h(\mathbf{K}\mathbf{w}_j) = \sum_{k=1}^{n} \beta_{jk} \mathbf{w}_k, \qquad j \in \{1, \ldots, n\}. \tag{61}$$

It is interesting to note that for each fixed j, the column vector $[\beta_{j1}, \ldots, \beta_{jn}]^T$ can be obtained by solving a small SPD linear system that has $G(\mathbf{w}_1, \ldots, \mathbf{w}_n)$ as the coefficient matrix and the jth column of $G_{\mathbf{K}}$ as the right-hand side.

(6) Computing elementwise numerical velocity. After a numerical pressure p_h is obtained, we compute its discrete weak gradient and assume

$$\nabla_{w,d} p_h = \sum_{j=1}^{n} \alpha_j \mathbf{w}_j.$$

Then we have an elementwise numerical velocity

$$\begin{aligned} \mathbf{u}_h &= \mathbf{Q}_h\left(-\mathbf{K}\nabla_{w,d} p_h\right) = -\sum_{j=1}^{n} \alpha_j \mathbf{Q}_h(\mathbf{K}\mathbf{w}_j) \\ &= -\sum_{k=1}^{n}\left(\sum_{j=1}^{n} \alpha_j \beta_{jk}\right)\mathbf{w}_k = \sum_{k=1}^{n} \gamma_k \mathbf{w}_k, \end{aligned} \tag{62}$$

which is attributed to elementwise matrix multiplication.

(7) Computing bulk normal fluxes. Instead of using a quadrature for evaluating the bulk normal flux defined in (21), we use the above formula and formula (15) section 2.2 to obtain

$$\int_{e_j \in E^\partial} \mathbf{u}_h \cdot \mathbf{n}_j = \sum_{k=1}^{n} \gamma_k \left(\int_{e_j \in E^\partial} \mathbf{w}_k \cdot \mathbf{n}_j \right) = \gamma_j |e_j|, \qquad 1 \le j \le n.$$

A similar technique can be used to evaluate elementwise numerical divergence.

(8) Vectorized assembly in MATLAB. A new aspect of finite element solvers on polygonal meshes is that the polygon type (quadrilaterals, pentagons, hexagons, etc.) varies. Accordingly, the element stiffness matrix size varies. Implementation in C++ would not be an issue, since C++ polymorphism and instantiation can be utilized. Implementation in MATLAB would be different, since vectorization for the entire mesh cannot be performed directly. Elementwise assembly would be inefficient. On the other hand, for a practical polygonal mesh, like one generated by `PolyMesher`, the polygons are mainly quadrilaterals, pentagons, hexagons, and 7-gons. In other words, the number of types is limited. With this consideration, our MATLAB implementation does the following:

(i) It retrieves mesh info on the maximal size (number of edges) of polygons.
(ii) It organizes the element stiffness matrices according to this maximum, and unoccupied entries are set to zero.
(iii) It performs vectorized assembly using the above data structure.

More details can be found in our MATLAB package `DarcyLite`.

(9) Schur complement or static condensation. Note the for this WG method, there are two groups of basis functions: one for the element interiors and the other for edges. For convenience, we use x_0 to denote the degrees of freedom associated with the former and x_1 for the latter. Then the assembled discrete linear system takes the following form:

$$\begin{bmatrix} A_{00} & A_{01} \\ A_{10} & A_{11} \end{bmatrix} \begin{bmatrix} x_0 \\ x_1 \end{bmatrix} = \begin{bmatrix} b_0 \\ b_1 \end{bmatrix}, \tag{63}$$

where A_{00} is a block diagonal matrix, since the interior basis functions for two different elements do not interact. Algebraically, we can apply the Schur complement technique. The element interior unknowns x_0 can be eliminated, and we solve a smaller size linear system for x_1 only, namely

$$\left(A_{11} - \left(A_{10}A_{00}^{-1}\right) A_{01}\right) x_1 = b_1 - \left(A_{10}A_{00}^{-1}\right) b_0. \tag{64}$$

Then x_0 is recovered as

$$x_0 = A_{00}^{-1}\left(b_0 - A_{01}x_1\right). \tag{65}$$

This technique shares the same spirit as those used in [30, 31] and reveals that static condensation [11] applies to this WG method also.

7. Numerical experiments. This section presents numerical results to demonstrate the accuracy and efficiency of the lowest-order WG solver on convex polygonal meshes. Three types of meshes are used in numerical tests, as shown in Figure 6.

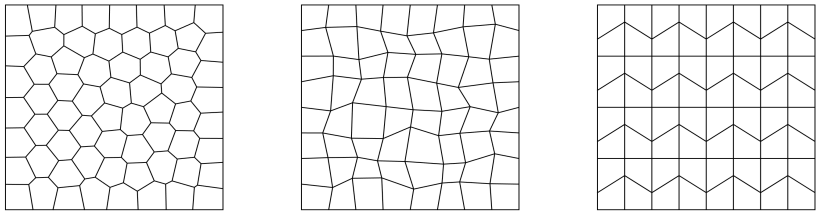

FIG. 6. *Three types of meshes used in numerical experiments.* Left: *a polygonal mesh generated by* `PolyMesher`. Middle: *a randomly h-perturbed quadrilateral mesh.* Right: *a trapezoidal mesh studied in* [2].

Example 1. This example is adopted from [26] with $\Omega = (0,1)^2$ and $\mathbf{K} = xy\,\mathbf{I}_2$. A known exact solution is $p(x,y) = x(1-x)y(1-y)$. Accordingly, the velocity is

$$\mathbf{u}(x,y) = [-x(1-2x)y^2(1-y), -x^2(1-x)y(1-2y)]^T,$$

and $f(x,y) = -(1-4x)y^2(1-y) - x^2(1-x)(1-4y)$. A homogeneous Dirichlet boundary condition is specified on the bottom, top, and left boundaries, whereas a Neumann boundary condition is specified on the right boundary. Shown in Tables 1 and 2 and Figure 7 are WG results.

TABLE 1
Example 1: *Results of* $WG(P_0, P_0; CW_0)$ *on polygonal meshes generated by* `PolyMesher`.

#Elem	h	$\|p - p_h^\circ\|$	Rate	$\|\mathbf{u} - \mathbf{u}_h\|$	Rate	$\|(\mathbf{u} - \mathbf{u}_h)\cdot\mathbf{n}\|$	Rate
$(2^3)^2$	1.89E-1	5.780E-3	–	5.651E-3	–	9.177E-3	–
$(2^4)^2$	9.23E-2	2.700E-3	1.09	2.394E-3	1.23	4.221E-3	1.12
$(2^5)^2$	4.57E-2	1.335E-3	1.01	1.004E-3	1.25	1.879E-3	1.16
$(2^6)^2$	2.28E-2	6.684E-4	0.99	4.661E-4	1.10	8.709E-4	1.10

TABLE 2
Example 1: *Results of* $WG(P_0, P_0; CW_0)$ *on randomly h-perturbed quadrilateral meshes.*

h	$\|p - p_h^\circ\|$	Rate	$\|\mathbf{u} - \mathbf{u}_h\|$	Rate	$\|(\mathbf{u} - \mathbf{u}_h) \cdot \mathbf{n}\|$	Rate
$1/2^3$	5.7065E-3	–	6.8578E-3	–	9.9357E-3	–
$1/2^4$	2.8499E-3	1.00	3.6151E-3	0.92	5.0437E-3	0.97
$1/2^5$	1.4276E-3	0.99	1.8198E-3	0.99	2.4787E-3	1.02
$1/2^6$	7.0955E-4	1.00	9.2219E-4	0.98	1.2450E-3	0.99
$1/2^7$	3.5357E-4	1.00	4.6155E-4	0.99	6.2157E-4	1.00

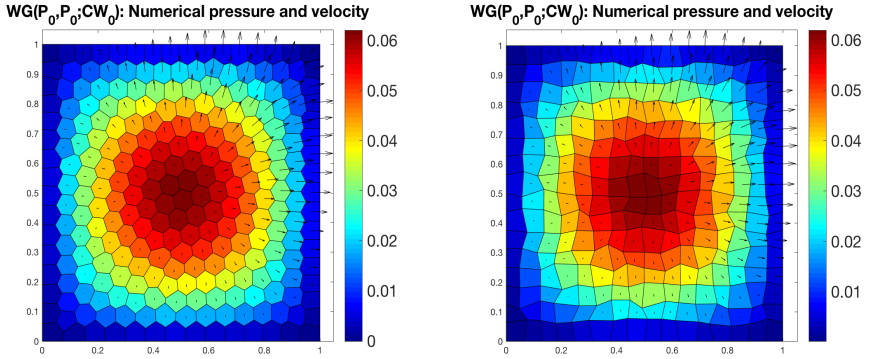

FIG. 7. *Example* 1: $WG(P_0, P_0; CW_0)$ *numerical pressure and velocity with* $h = \frac{1}{16}$. Left: *on a polygonal mesh generated by* `PolyMesher`. Right: *on a randomly h-perturbed quadrilateral mesh.*

Example 2. This is a frequently tested example with $\Omega = (0,1)^2$, $\mathbf{K} = \mathbf{I}_2$, a known exact solution $p(x,y) = \sin(\pi x)\sin(\pi y)$, and a homogeneous Dirichlet boundary condition on the whole boundary. We test the $\mathrm{WG}(P_0, P_0; CW_0)$ solver developed in this paper, the penalized $\mathrm{WG}(P_1, P_0; P_0^2)$ solver derived from [25], and the CG-type solver in [19] on a sequence of trapezoidal meshes introduced in [2].

As shown in Table 3, the new $\mathrm{WG}(P_0, P_0; CW_0)$ solver has first-order convergence in both pressure and velocity, as proved in section 4. The penalized $\mathrm{WG}(P_1, P_0; P_0^2)$ has second-order convergence in pressure, since linear polynomials are used inside elements. Velocity was not discussed in [25]. The CG method with the Wachspress coordinates [19] uses the least unknowns and has, respectively, first- and second-order convergence in pressure and velocity. However, this CG method is not locally conservative, nor does it produce a continuous normal flux. As investigated in [28], an elementwise residual of local mass conservation can be defined as

$$\mathcal{R}_h(E) = \int_E f - \int_{E^\partial} \mathbf{u}_h \cdot \mathbf{n} \qquad \forall E \in \mathcal{E}_h, \tag{66}$$

where $\mathbf{u}_h$ is the numerical velocity. Shown in Figure 8 are a profile of the elementwise residual along with a plot of the normal flux difference across all edges, both for the trapezoidal mesh with $h = 1/16$.

Example 3. This example is adopted from page 918 in [2]. Here $\Omega = (0,1)^2$ and $\mathbf{K} = \mathbf{I}_2$. The exact solution is a polynomial $p(x,y) = x^3 + 5y^2 - 10y^3 + y^4$. Accordingly, $f(x,y) = -(6x + 10 - 60y + 12y^2)$. A Dirichlet boundary condition is specified on the whole boundary.

TABLE 3
Example 2: *Results of three numerical methods on trapezoidal meshes.*

	WG($P_0, P_0; CW_0$)		WG($P_1, P_0; P_0^2$) Penalty $\rho = 1$	CG Wachspress	
h	$\|p - p_h^\circ\|$	$\|\mathbf{u} - \mathbf{u}_h\|$	$\|p - p_h^\circ\|$	$\|p - p_h\|$	$\|\mathbf{u} - \mathbf{u}_h\|$
$1/2^3$	8.339E-2	2.743E-1	6.616E-2	1.271E-2	3.202E-1
$1/2^4$	4.181E-2	1.385E-1	1.667E-2	3.227E-3	1.610E-1
$1/2^5$	2.092E-2	6.971E-2	4.183E-3	8.098E-4	8.066E-2
$1/2^6$	1.046E-2	3.497E-2	1.047E-3	2.026E-4	4.035E-2
$1/2^7$	5.231E-3	1.752E-2	2.620E-4	5.067E-5	2.017E-2
Rate	0.998	0.992	1.995	1.992	0.997

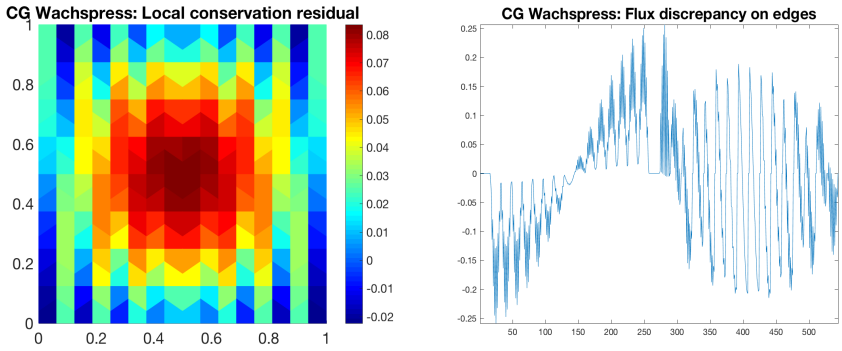

FIG. 8. *Example* 2: *continuous Galerkin finite element method with the Wachspress coordinates as Lagrangian-type basis functions,* $h = 1/16$. Left: *elementwise residual of local mass conservation.* Right*: normal flux discrepancy across all edges.*

TABLE 4
Example 3: *Superconvergence of* $\|p_h^\circ - Q_h^\circ p\|$ *and first-order convergence in div on randomly* h*-perturbed quadrilateral meshes.*

h	$\|p_h^\circ - Q_h^\circ p\|$	Rate	$\mathrm{div}(\mathbf{u} - \mathbf{u}_h)$	Rate
$1/2^3$	2.3515E-3	–	1.8171E-0	–
$1/2^4$	6.4020E-4	1.87	9.1842E-1	0.98
$1/2^5$	1.6776E-4	1.93	4.6157E-1	0.99
$1/2^6$	4.4475E-5	1.91	2.3061E-1	1.00
$1/2^7$	1.1364E-5	1.96	1.1527E-1	1.00

For this example, we examine superconvergence in the discrete error $\|p_h^\circ - Q_h^\circ p\|$, as discussed at the end of subsection 4.5. As shown in Table 4, close to second-order convergence occurs even for a family of randomly h-perturbed quadrilateral meshes. Furthermore, first-order convergence is observed for errors in div of velocity.

8. Concluding remarks. In this paper, we have developed a novel WGFEM for solving Darcy flow problems on convex polygonal meshes. This new method utilizes the Wachspress coordinates along with the Chen–Wang $H(\mathrm{div})$-subspaces within the WG framework. This new solver is cost-effective, since only one unknown is needed per cell or per edge. The cell unknowns can be eliminated via Schur complement or static condensation. The main features of this new method are as follows:

(i) It is applicable to general convex polygonal meshes.
(ii) It results in symmetric positive-definite sparse linear systems.
(iii) There is no need for penalization.
(iv) It has just constant approximants and hence is easy to use.
(v) It has local mass conservation.
(vi) It has flux normal continuity.
(vii) It has optimal-order convergence in pressure, velocity, and normal flux on shape-regular meshes.

The WG methodology can be extended to elliptic problems on polyhedral meshes. This is tightly related to the Chen–Wang $H(\mathrm{div})$-finite elements on polyhedra [9]. The 3-dim version could be implemented more efficiently by utilizing C++ polymorphism to handle various types of polyhedra. This is currently being investigated and will be reported in our future work.

REFERENCES

[1] T. Arbogast and M. R. Correa, *Two families of mixed finite elements on quadrilaterals of minimal dimension*, SIAM J. Numer. Anal., 54 (2016), pp. 3332–3356, https://doi.org/10.1137/15M1013705.

[2] D. Arnold, D. Boffi, and R. Falk, *Approximation by quadrilateral finite elements*, Math. Comp., 71 (2002), pp. 909–922.

[3] D. Arnold, D. Boffi, and R. S. Falk, *Quadratic $H(\mathrm{div})$ finite elements*, SIAM J. Numer. Anal., 42 (2005), pp. 2429–2451, https://doi.org/10.1137/S0036142903431924.

[4] F. Brezzi and M. Fortin, *Mixed and Hybrid Finite Element Methods*, Springer-Verlag, 1991.

[5] F. Brezzi, K. Lipnikov, and M. Shashkov, *Convergence of the mimetic finite difference method for diffusion problems on polyhedral meshes*, SIAM J. Numer. Anal., 43 (2005), pp. 1872–1896, https://doi.org/10.1137/040613950.

[6] L. Bush and V. Ginting, *On the application of the continuous Galerkin finite element method for conservation problems*, SIAM J. Sci. Comput., 35 (2013), pp. A2953–A2975, https://doi.org/10.1137/120900393.

[7] A. Cangiani, E. Georgoulis, and P. Houston, *hp-version discontinuous Galerkin methods on polygonal and polyhedral meshes*, Math. Models Methods Appl. Sci., 24 (2014), pp. 2009–2041.

[8] L. Chen, J. Wang, and X. Ye, *A posteriori error estimates for weak Galerkin finite element methods for second order elliptic problems*, J. Sci. Comput., 59 (2014), pp. 496–511.

[9] W. Chen and Y. Wang, *Minimal degree $H(\mathrm{curl})$ and $H(\mathrm{div})$ conforming finite elements on polytopal meshes*, Math. Comp., 86 (2017), pp. 2053–2087.

[10] P. Ciarlet, *The Finite Element Method for Elliptic Problems*, SIAM, 2002, https://doi.org/10.1137/1.9780898719208.

[11] B. Cockburn, *Static condensation, hybridization, and the devising of the HDG methods*, in Building Bridges: Connection and Challenges in Modern Approaches to Numerical Partial Differential Equations, Springer, 2016, pp. 129–177.

[12] B. Cockburn, D. A. DiPietro, and A. Ern, *Bridging the hybrid high-order and hybridizable discontinuous Galerkin methods*, ESAIM Math. Model. Numer. Anal., 50 (2016), pp. 635–650.

[13] L. B. DaVeiga, F. Brezzi, D. Marini, and A. Russo, *$H(\mathrm{div})$ and $H(\mathrm{curl})$-conforming virtual element methods*, Numer. Math., 133 (2016), pp. 303–332.

[14] L. B. DaVeiga, F. Brezzi, D. Marini, and A. Russo, *Virtual element method for general second-order elliptic problems on polygonal meshes*, Math. Models Methods Appl. Sci., 26 (2016), pp. 729–750.

[15] J. Droniou, R. Eymard, T. Gallouët, and R. Herbin, *A unified approach to mimetic finite difference, hybrid finite volume and mixed finite volume methods.*, Math. Models Methods Appl. Sci., 20 (2010), pp. 265–295.

[16] J. Droniou, R. Eymard, and R. Herbin, *Gradient schemes: Generic tools for the numerical analysis of diffusion equations*, ESAIM Math. Model. Numer. Anal., 50 (2016), pp. 749–781.

[17] R. Eymard, T. Gallouët, and R. Herbin, *Discretization of heterogeneous and anisotropic diffusion problems on general nonconforming meshes SUSHI: A scheme using stabilization*

and hybrid interfaces, IMA J. Numer. Anal., 30 (2010), pp. 1009–1043.
[18] R. Falk, P. Gatto, and P. Monk, *Hexahedral H(div) and H(curl) finite elements*, ESAIM Math. Model. Numer. Anal., 45 (2011), pp. 115–143.
[19] M. Floater, A. Gillette, and N. Sukumar, *Gradient bounds for Wachspress coordinates on polytopes*, SIAM J. Numer. Anal., 52 (2014), pp. 515–532, https://doi.org/10.1137/130925712.
[20] A. Gillette, A. Rand, and C. Bajaj, *Construction of scalar and vector finite element families on polygonal and polyhedral meshes*, Comput. Methods Appl. Math., 16 (2016), pp. 667–683.
[21] V. Gyrya and K. Lipnikov, *High-order mimetic finite difference method for diffusion problems on polygonal meshes*, J. Comput. Phys., 227 (2008), pp. 8841–8854.
[22] G. Lin, J. Liu, L. Mu, and X. Ye, *Weak Galerkin finite element methods for Darcy flow: Anisotropy and heterogeneity*, J. Comput. Phys., 276 (2014), pp. 422–437.
[23] G. Lin, J. Liu, and F. Sadre-Marandi, *A comparative study on the weak Galerkin, discontinuous Galerkin, and mixed finite element methods*, J. Comput. Appl. Math., 273 (2015), pp. 346–362.
[24] J. Liu, S. Tavener, and Z. Wang, *The lowest-order weak Galerkin finite element methods for the Darcy equation on quadrilateral and hybrid meshes*, J. Comput. Phys., 359 (2018), pp. 312–330.
[25] L. Mu, J. Wang, and X. Ye, *A weak Galerkin finite element method with polynomial reduction*, J. Comput. Appl. Math., 285 (2015), pp. 45–58.
[26] L. Mu, J. Wang, and X. Ye, *Weak Galerkin finite element methods on polytopal meshes*, Int. J. Numer. Anal. Model., 12 (2015), pp. 31–53.
[27] B. Riviere, *Discontinuous Galerkin Methods for Solving Elliptic and Parabolic Equations: Theory and Implementation*, SIAM, 2008, https://doi.org/10.1137/1.9780898717440.
[28] S. Sun and J. Liu, *A locally conservative finite element method based on piecewise constant enrichment of the continuous Galerkin method*, SIAM J. Sci. Comput., 31 (2009), pp. 2528–2548, https://doi.org/10.1137/080722953.
[29] C. Talischi, G. Paulino, A. Pereira, and I. Menezes, `PolyMesher`*: A general-purpose mesh generator for polygonal elements written in Matlab*, Struct. Multidiscip. Optim., 45 (2012), pp. 309–328.
[30] M. Vohralik and B. Wohlmuth, *From face to element unknowns by local static condensation with application to nonconforming finite elements*, Comput. Methods Appl. Mech. Engrg., 253 (2013), pp. 517–529.
[31] M. Vohralik and B. Wohlmuth, *Mixed finite element methods: Implementation with one unknown per element, local flux expressions, positivity, polygonal meshes, and relations to other methods*, Math. Models Methods Appl. Sci., 23 (2013), pp. 803–838.
[32] E. Wachspress, *A Rational Finite Element Basis*, Math. Sci. Eng. 114, Academic Press, 1975.
[33] E. Wachspress, *Barycentric coordinates for polytopes*, Comput. Math. Appl., 61 (2011), pp. 3319–3321.
[34] C. Wang and J. Wang, *An efficient numerical scheme for the biharmonic equation by weak Galerkin finite element methods on polygonal or polyhedral meshes*, Comput. Math. Appl., 68 (2014), pp. 2314–2330.
[35] J. Wang and X. Ye, *A weak Galerkin finite element method for second order elliptic problems*, J. Comput. Appl. Math., 241 (2013), pp. 103–115.
[36] J. Wang and X. Ye, *A weak Galerkin mixed finite element method for second order elliptic problems*, Math. Comp., 83 (2014), pp. 2101–2126.
[37] M. F. Wheeler, G. Xue, and I. Yotov, *A multipoint flux mixed finite element method on distorted quadrilaterals and hexahedra*, Numer. Math., 121 (2012), pp. 165–204.
[38] M. F. Wheeler and I. Yotov, *A multipoint flux mixed finite element method*, SIAM J. Numer. Anal., 44 (2006), pp. 2082–2106, https://doi.org/10.1137/050638473.
[39] S. Zhang, *On the nested refinement of quadrilateral and hexahedral finite elements and the affine approximation*, Numer. Math., 98 (2004), pp. 559–579.